CHAPTER IV
RESULTS AND DISCUSSION

4.1 Particle Size Distribution of NR Latex

The particle size distribution curve of NR latex particles is shown in Figure 4.1 with mean diameter 0.97±0.10 μm and the mean specific surface area 7.46±0.78 m^2/g. These results indicate the polydispersity of NR latex particles with narrow size distribution.

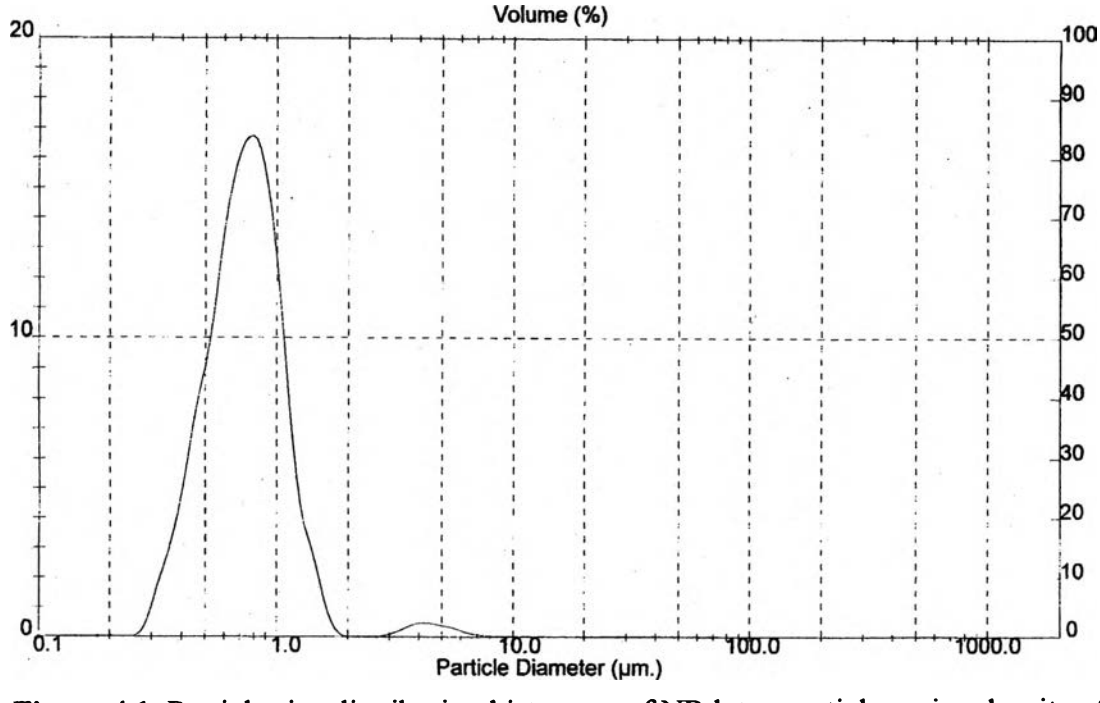

Figure 4.1 Particle size distribution histogram of NR latex particles using density of NR particle = 1 g/cm^3 whereas typical density of NR ~ 0.93 g/cm^3 (Long, H., 1985).

4.2 Admicelled Latex Films and Composites

Only admicelled latex polymerized from N2-1 to N2-4 and N3-1 to N3-3 can be cast into rubber sheet. The color of the films changed from transparent pale yellow to dark brown corresponding with increasing pyrrole concentration in the mixtures as shown in Figures 4.2 to 4.4 compared to the bare latex.

4.3 Optical Microscopy Study

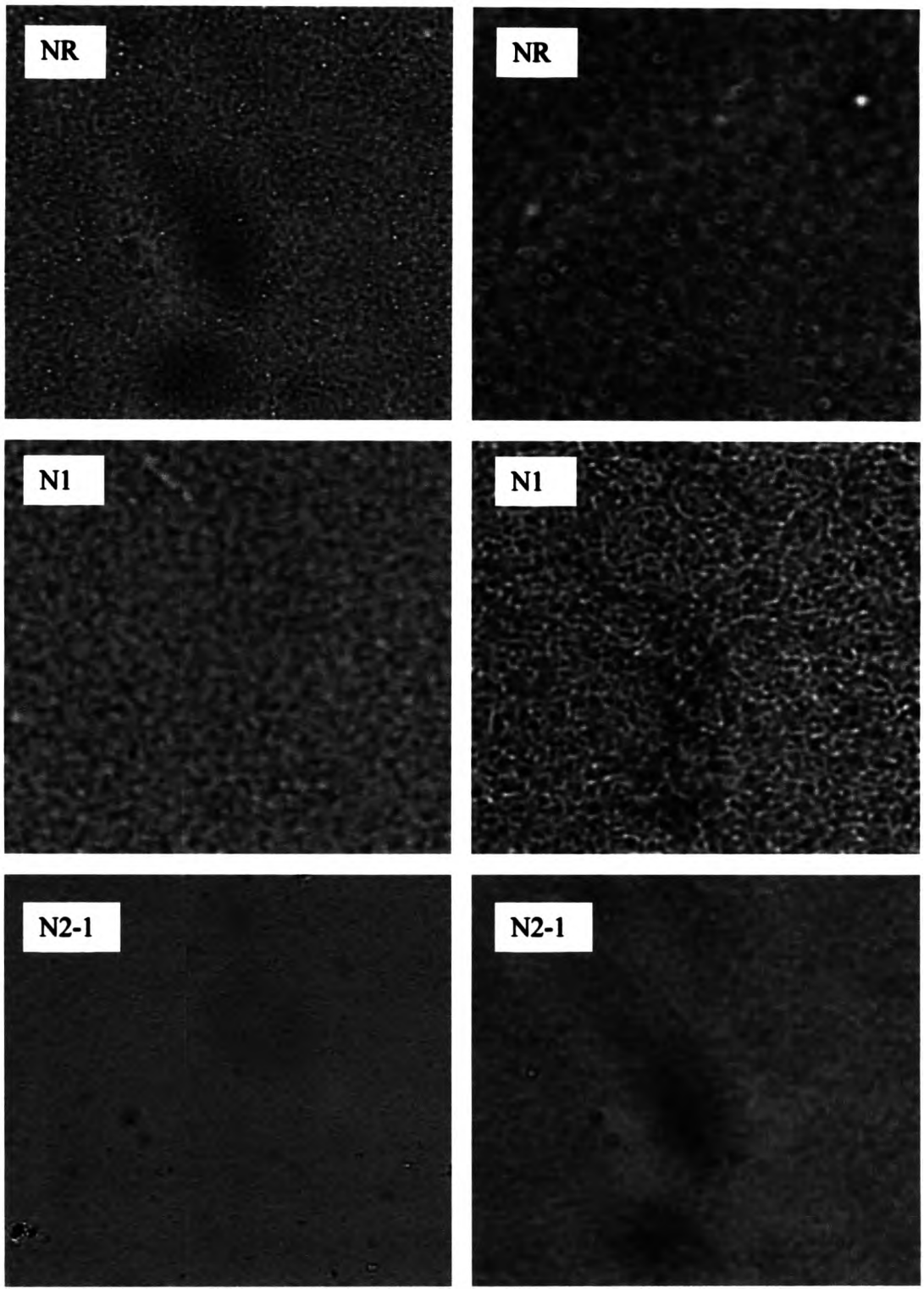

Figure 4.2 Optical micrographs of NR latex particles, N1, and N2-1 with 200 magnification in the left Figures and 500 magnifications in the right Figures (except NR, 500 and 1000 magnifications in the left and right Figures, respectively.)

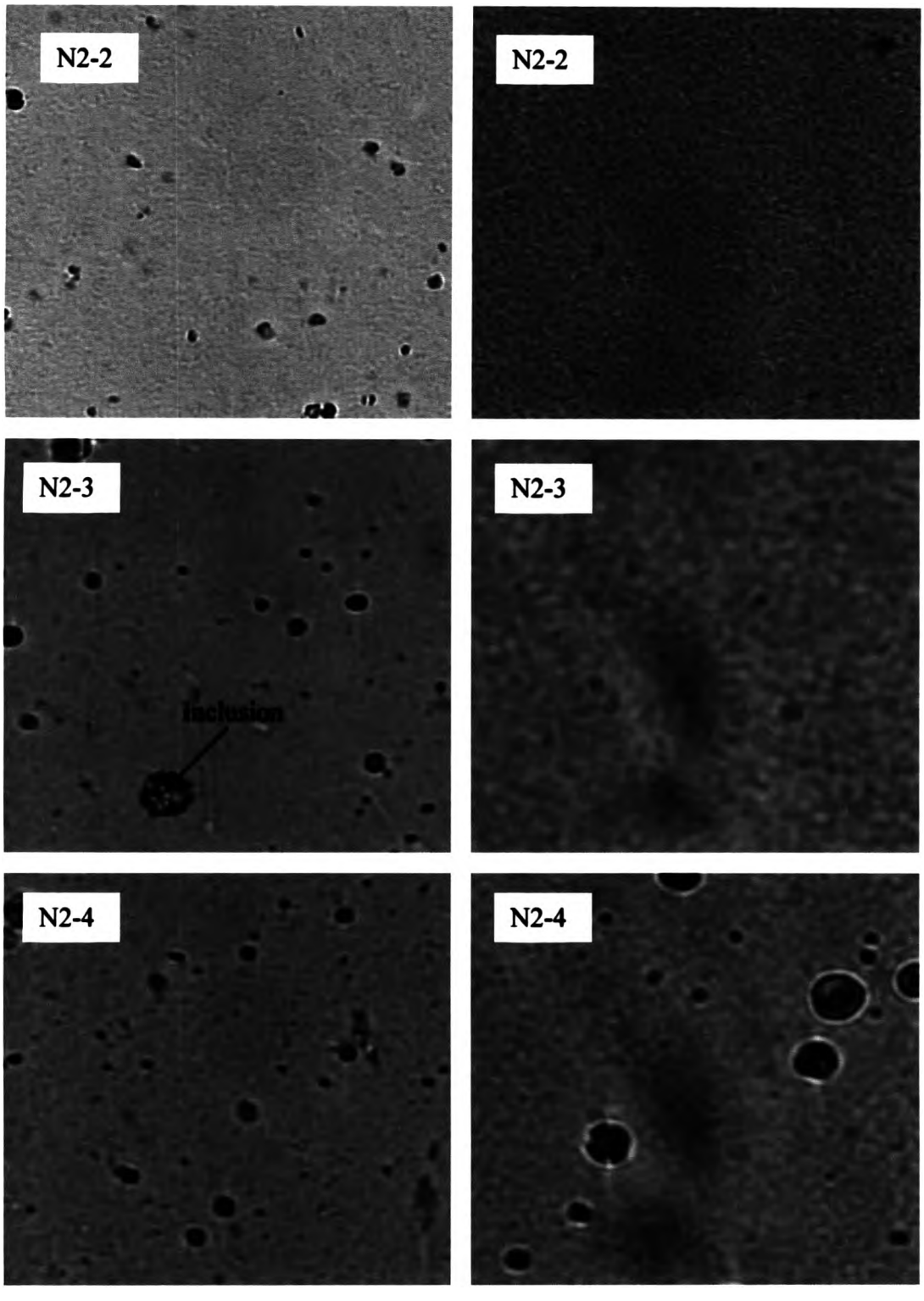

Figure 4.3 Optical micrographs of N2-2, N2-3, and N2-4 with 200 magnifications for the left Figures and 500 magnifications in the right Figures.

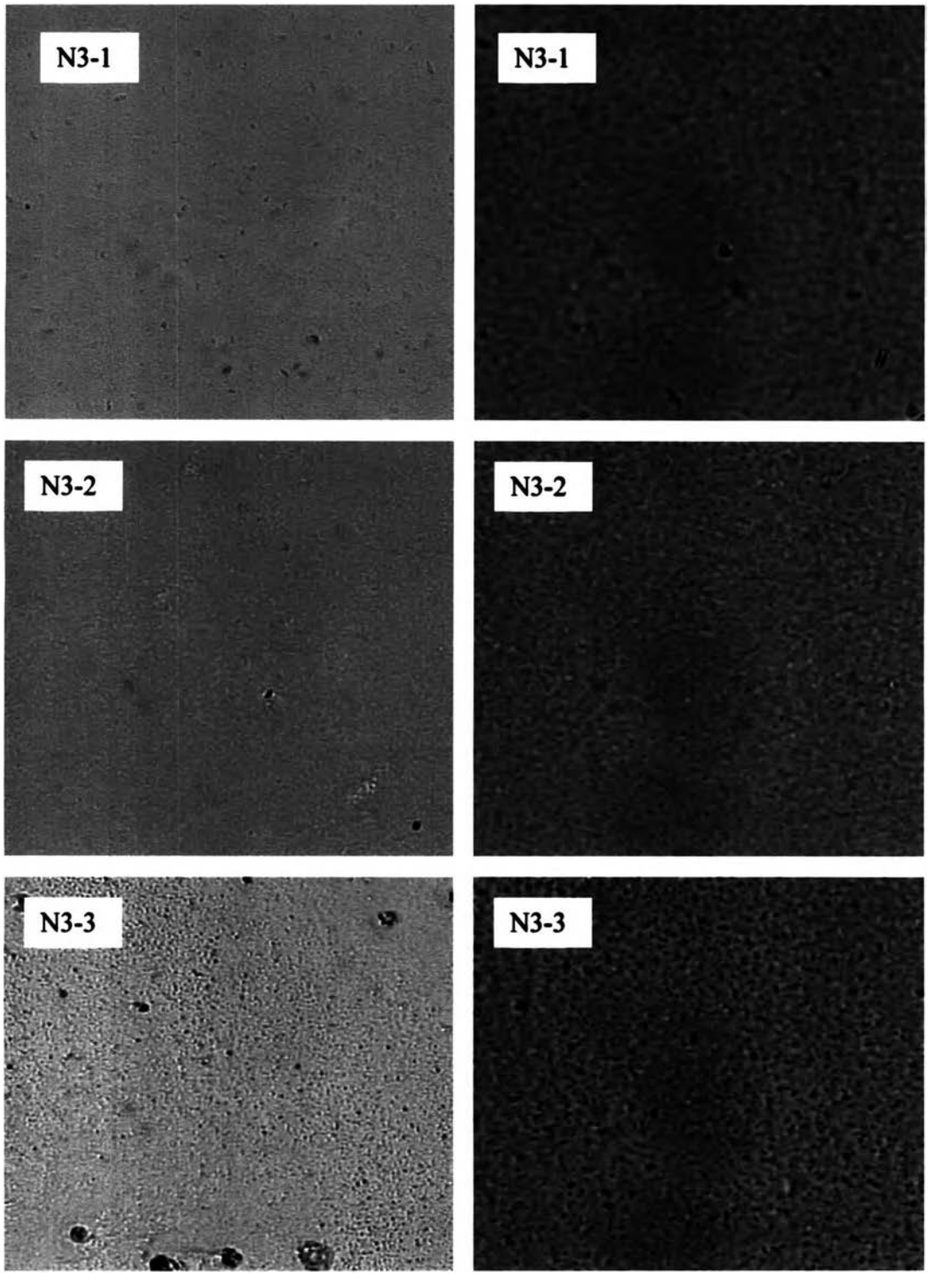

Figure 4.4 Optical micrographs of N3-1, N3-2, and N3-3 with 200 magnifications for the left Figures and 500 magnifications in the right Figures.

Figures 4.2-4.4 show optical micrographs of NR latex film and admicelled latex films containing different pyrrole concentrations. The pictures reveal that the texture of the film N2-1 is smoother than N1 which was not prepared by admicellar polymerization technique. The dark coverage area of PPy on NR latex particles can be seen in N1, N2, and N3 systems. The results are similar to those reported by Huijs *et al.* (2001) that the film transparency reduced with increasing PPy (from 100% without PPy to 50% with 4 wt% PPy). They also found that surfactant used to stabilize colloid reduced the transparency. Table 4.1 shows the colloidal stability of the latices after polymerization for both one and two-step. The micrograph of N2-1 (5 mM pyrrole) followed the adsolubilization curve of the previous work. If the more concentration of pyrrole was added, PPy could further be adsolubilized only slightly. The excess amount of pyrrole can be seen from the micrograph of N2-4. Phase separation occurred, PPy-rich phase can be clearly seen. However, there was also NR latex particles in PPy-rich phase. From these Figures, it could be noted that the coatings are uneven for the admicelled latex with excess concentration of pyrrole. The whole pyrrole was not used up for coating on NR latex surface, some monomers were self-polymerized resulting in PPy black particles embedded as the black phase. The more pyrrole concentration added, the more inhomogeneous of the rubber film. PPy dark phase of N3-3 is highest among N3-2 and N2-3. From the whole Figures, PPy dark phases in N3 system is obviously more densed and thicker than those in N2 system. This result can be explained that the addition of salt will help to reduce the repulsion between head groups of surfactants leading to higher amount of PPy adsolubilizates.

Table 4.1 Colloidal stability of the coated latices after polymerization

	Homogeneous liquid*	Inhomogeneous** liquid	Agglomeration
Sample codes	N1, Ctrl. 1, Ctrl. 2, N2-1 N2-2, N2-3, N3-1, N3-2	N2-4 and N3-3	N2-5, N3-4, N3-5, All samples obtained from 2-step mixing

*Homogeneous liquid = milky white NR latex mixtures, the color changed (into brown) with pyrrole concentration.

**Inhomogeneous liquid = NR latex mixture with a small agglomeration of PPy in the mixture, the color of the mixtures were brown.

4.4 Scanning Electron Microscopy

Figure 4.5 shows morphology of PPy having globular structure with its globule size around 4 μm/globule. The photomicrographs of admicelled latex/PPy composite from 2-step process (Figures 4.6-4.7) revealed phase separation of the composites. PPy is the bright phase segregated from NR dark phase. SEM images suggest that the particle surfaces in the samples were only partially covered with PPy (small globular agglomerates). At lower content of PPy, PPy was the dispersed phase in NR matrix and the phase inversion occurred in the higher amount of PPy (for samples that contain 90% by weight of PPy). When the PPy content was raised, evidence for PPy bright phase was enhanced as can be seen in sample N2-1A1P9. For the composition of 50/50, PPy aggregates are still distributed in NR matrix. Comparing between N2-1 and N2-2, more PPy particles was adhered to admicelled latex in N2-2 and the agglomerate size was reduced. This is a result of more PPy in sample N2-2 providing more miscible site for new PPy deposition. For sample N3, tiny particles of PPy distribute more evenly and densely and they agglomerate more than N2 system because of salt addition allowing more pyrrole adsolubilization.

Film formation became more difficult as PPy content increased due to the rigid PPy phase encapsulate the low glass transition temperature (soft) core. Morphology study by optical microscope was not convenient and thus SEM was employed for solid samples instead (Huijs *et al.*, 2001 and Lascelles and Armes, 1997). Submicrometer sized globular polypyrrole like bulk powder was found to form as a separate subphase in polystyrene/polypyrrole composite at high PPy content (51.1 wt%) and when PPy was coated at 25 wt% on micron sized polystyrene particles, globular polypyrrole overlayer was found. However, at low loading (<10wt%) smooth uniform PPy coating of 2-20 nm on polystyrene was seen by SEM (Lascelles and Armes, 1997). Bhat *et al.* (1995) also found globular structure of PPy

deposited on poly(vinylidene fluoride) or PVDF film. Li and Ouyang (2000) reported the big agglomerates of PPy on the film surface causing surface roughness for the sample without non-ionic surfactant. The fine-uniform dispersed phase with surface smoothness was obtained for sample prepared with surfactant.

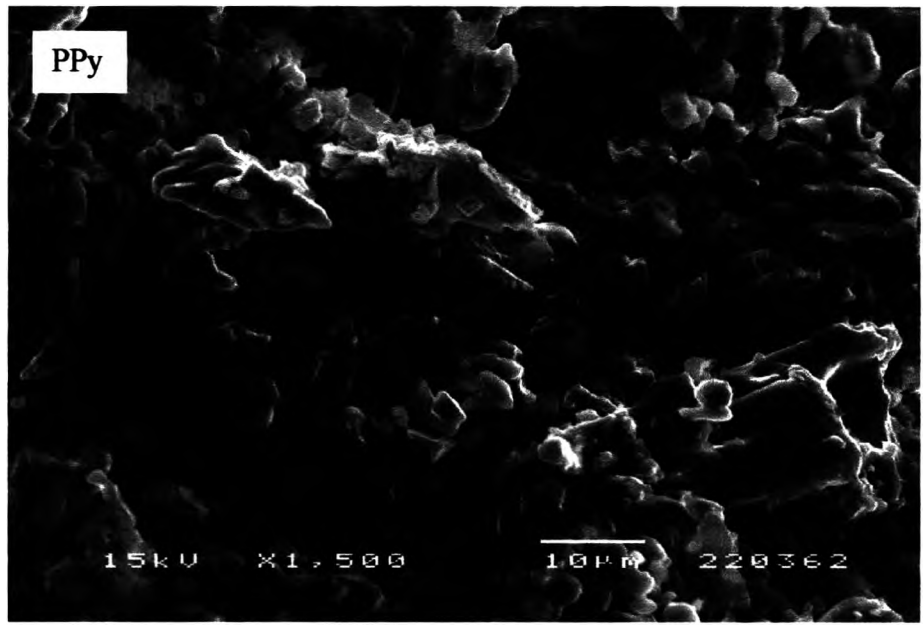

Figure 4.5 Scanning electron micrograph of PPy powder prepared from oxidative polymerization of pyrrole with ammonium persulfate at 30^0C for 4 hours.

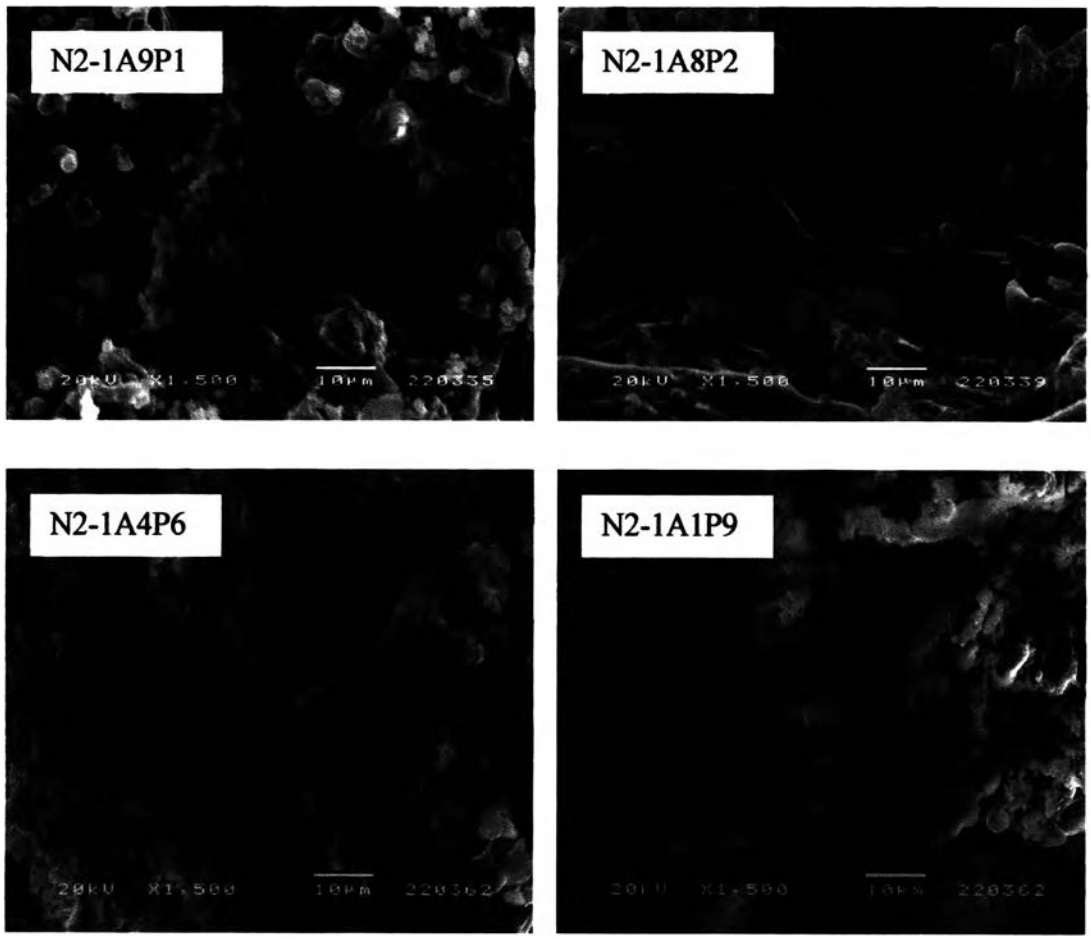

Figure 4.6 Scanning electron micrographs of admicelled latex (N2-1) mixed with 10wt% PPy (N2-1A9P1), 20 wt% PPy (N2-1A8P2), 60 wt%.PPy (N2-1A4P6), and 90wt% PPy (N2-1A1P9) by 2-step polymerization.

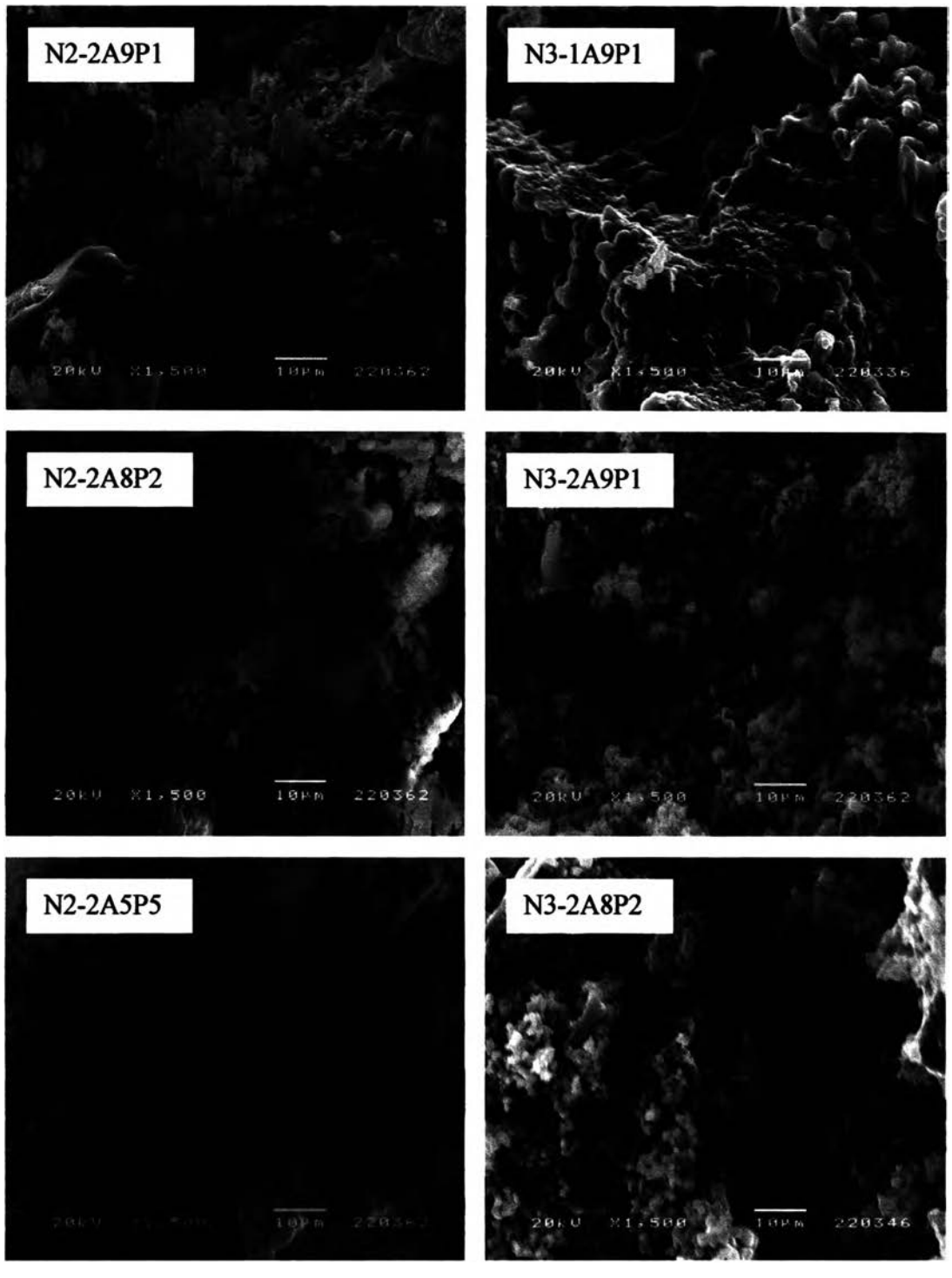

Figure 4.7 Scanning electron micrographs of admicelled latex (N2-2, N3-1, and N3-2) mixed with PPy at various content by 2-step polymerization.

4.5 Thermogravimetric Analysis

The samples of pure NR latex, PPy powder, and admicelled latices containing various amounts of PPy were studied by thermogravimetric analysis (TGA). Table 4.2 summarizes the results of TGA investigation. For chemically prepared PPy, the degradation temperature was observed at 264^{0}C (for the first region) and 341^{0}C for the second region as also seen in Figure 4.8. Oxygen atmosphere did not cause strong effect to PPy before 200^{0}C (The Figure was shown in Appendix C, Figure C-1). The degradation temperature of the controlled system followed a similar pattern to that of pure NR latex. However, PPy exerted a small stabilizing effect on the coated latices (N2, N3, and 2-step polymerization system) as can be seen from Figures 4.9-4.11. The thermal stability was shifted to higher temperatures with increasing PPy content. The decomposition maximum increased from 365^{0}C for pure NR latex to 374^{0}C for N2-5 (60 mM pyrrole) but no significant changes in thermal stability of N2-1 to N2-4 as shown in Figure 4.9. Figure 4.10 represents the thermograms of admicelled latex with adding salt, the degradation temperature was a little higher than N2 system. The thermal stability of NR/PPy composites made from 2-step polymerization increased with increasing PPy content as shown in Figure 4.11. But at low PPy content, thermal properties was close to those of the admicelled samples. In contrast to two-step process, one-step polymerization brings about much better homogeneous samples showing only one degradation temperature like admicelled sample while two-step polymerization shows heterogeneity of the two phases as seen from two degradation peaks like those of pure PPy. Thermograms of two-step polymerization made of N3-2 shows better thermostability with higher residue content than that made of N2-2. Omastova *et al.* (1997) reported thermal stability of PPy coated PMMA (>390^{0}C) is enhanced compared to pure PMMA (385^{0}C) and more residue remaining as PPy content increases.

Table 4.2 Thermostability results (under nitrogen atmosphere) from TGA analysis (TGA furnace = 20 ml/min., TGA balance = 30 ml/min.)

Sample	Region	On set temp. (^{0}C)	End point temp. (^{0}C)	Peak temp. (^{0}C)	Mass loss (%)
PPy powder	A	229.64	270.60	263.97	18.81
	B	270.60	356.57	340.99	39.83
NR latex*	A	340.85	385.57	364.65	98.79
Ctrl. 1	A	345.39	388.88	369.18	98.79
Ctrl. 2	A	345.48	390.19	369.28	99.63
N1	A	343.30	390.90	369.27	99.65
N2-1	A	346.07	390.06	368.43	99.76
N2-2	A	346.09	390.08	368.44	99.36
N2-3	A	344.75	391.63	368.55	99.98
N2-4	A	345.42	392.29	368.50	99.98
N2-5	A	346.86	402.38	373.54	96.76
N3-1	A	344.74	390.18	369.26	99.11
N3-2	A	344.99	390.06	368.98	99.28
N3-3	A	345.39	390.10	369.19	100.28
N3-4	A	348.94	399.42	371.30	97.39
N3-5	A	345.52	398.16	372.20	92.90
N2-1A1P9_2	A	223.10	265.89	259.16	21.29
	B	265.89	348.58	334.64	39.09
N2-2A9P1_1#	A	346.81	390.80	369.89	99.67
N2-2A9P1_2	A	228.56	270.39	258.85	24.96
	B	350.43	400.20	369.90	52.92
N2-2A5P5_2	A	224.68	267.59	260.02	26.92
	B	267.59	335.38	320.96	38.75
N2-2A8P2_2	A	233.53	282.57	271.03	33.97
	B	282.57	397.95	367.02	53.97
N3-2A9P1_2	A	346.17	404.58	367.80	88.82

*Pure NR latex after purification without $(NH_4)_2S_2O_8$

#From the same formula for N2-2 but add more pure pyrrole (not solution) up to total weight of 10%

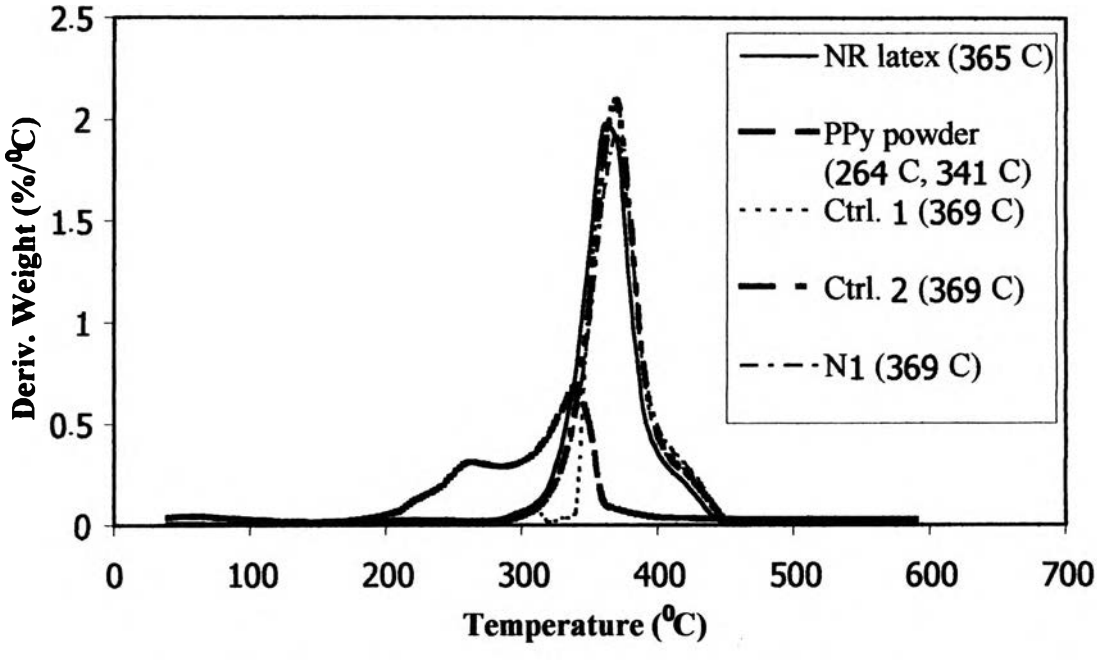

Figure 4.8 DTGA thermograms of NR latex film, PPy powder, Ctrl. 1, Ctrl. 2, and N1.

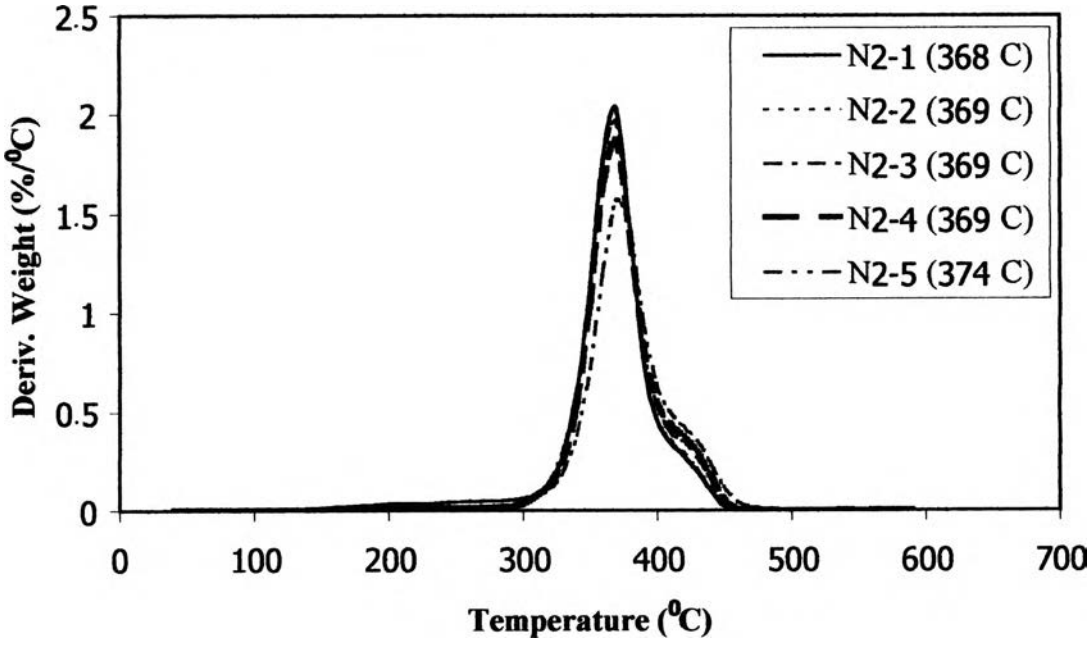

Figure 4.9 DTGA thermograms of admicelled latex films without salt addition.

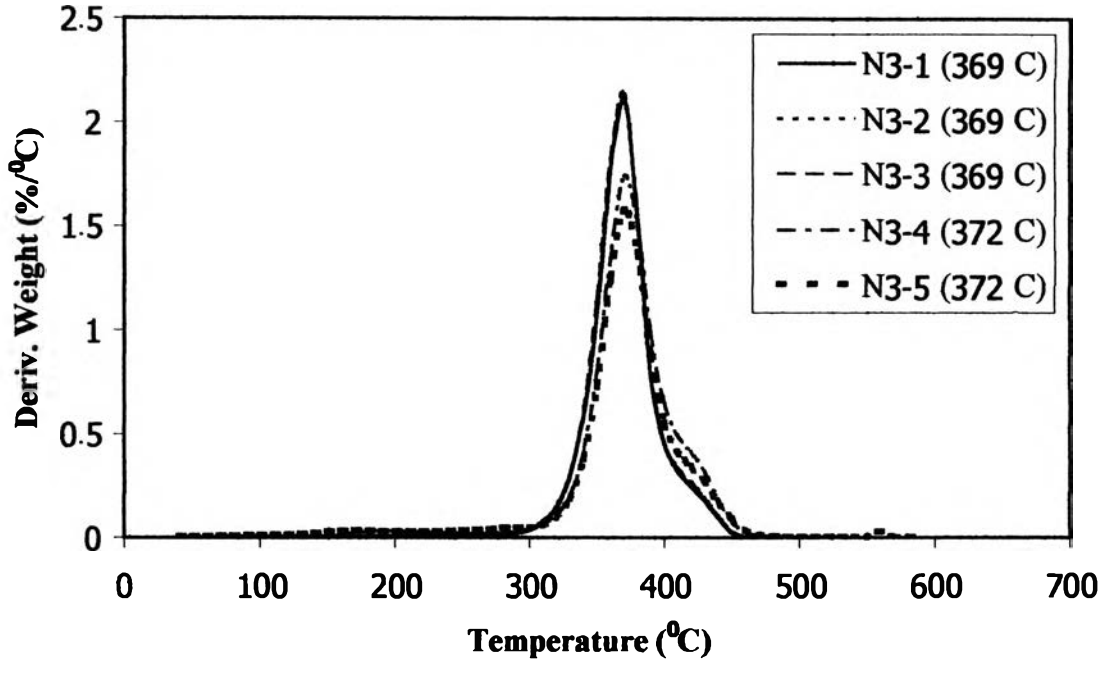

Figure 4.10 DTGA thermograms of admicelled latex films with salt addition.

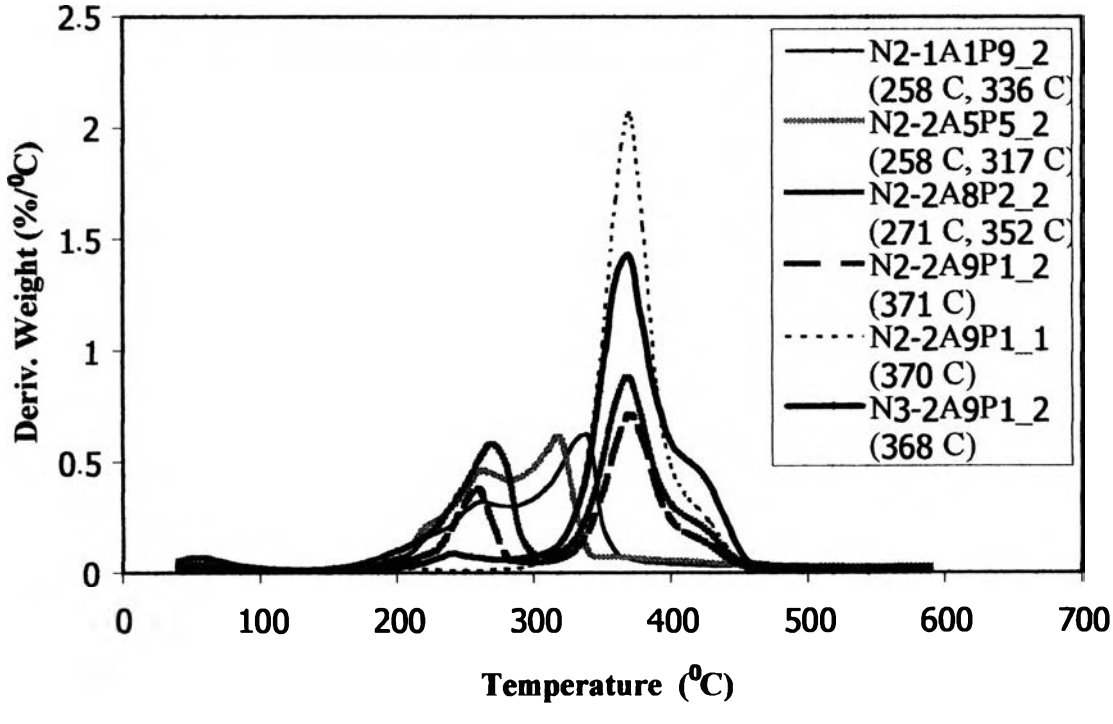

Figure 4.11 DTGA thermograms of admicelled latex obtained by two-step polymerization.

4.6 Fourier-Transform Infrared Spectroscopy of admicelled NR latex

Results from FTIR are shown in Figures 4.12-4.14. The IR spectra of pure NR latex, SDS and Ctrl. 1 are shown in Figure 4.12 suggesting the presence of both NR and SDS in Ctrl. 1. Pure PPy IR spectrum is presented in Figure 4.13. The characteristic peaks of PPy are at 1557, 1182, 1035, and 786 cm^{-1}. The peak of about 1600-1650 cm^{-1} results from ring vibration of PPy and the peak position around 1035 cm^{-1} represents C-H and N-H stretching of PPy. The obtained spectra correlate closely with the IR spectra of PPy reported by Omastova, M., *et al.*, 1998. From Figure 4.14, the spectra of N1, N2-1, and N3-1 represent the combinated chemistry of NR latex and PPy (5 mM). Such that there are no band positions that are belonged to pyrrole (The Aldrich Library of FT-IR Spectra, edition II, vol. 3, 3408). The number above each peak represents the band positions for PPy. These results confirm the polymerization of pyrrole to PPy or PPy exists after polymerization.

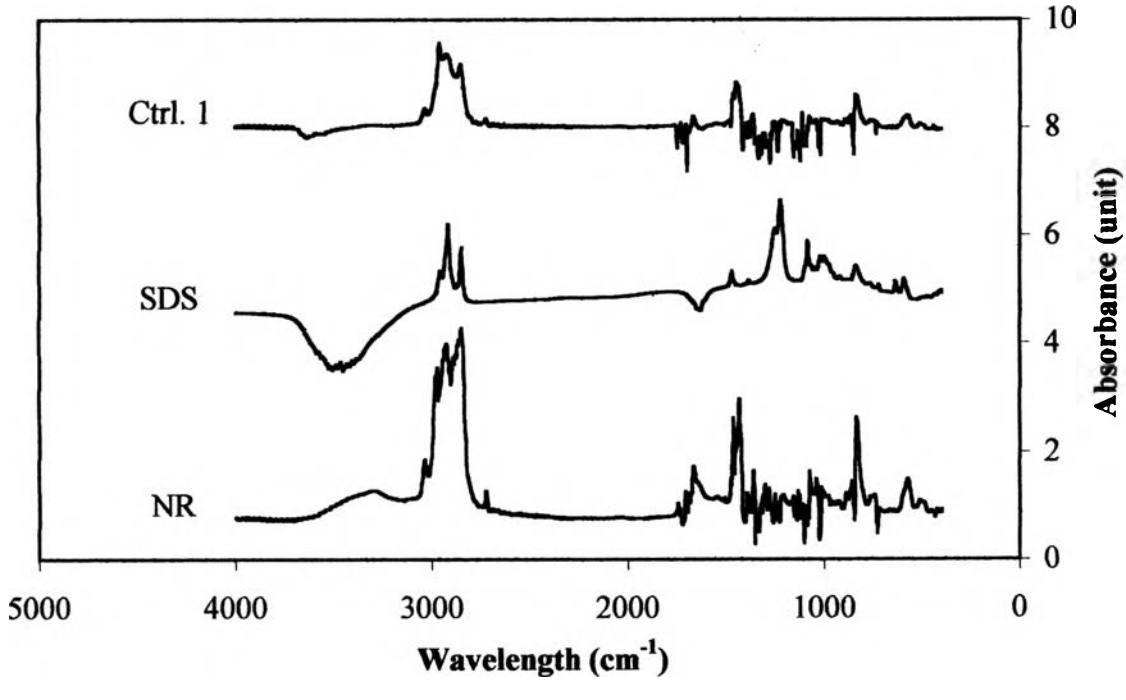

Figure 4.12 FT-IR spectra of pure NR latex film, SDS, and Ctrl. 1.

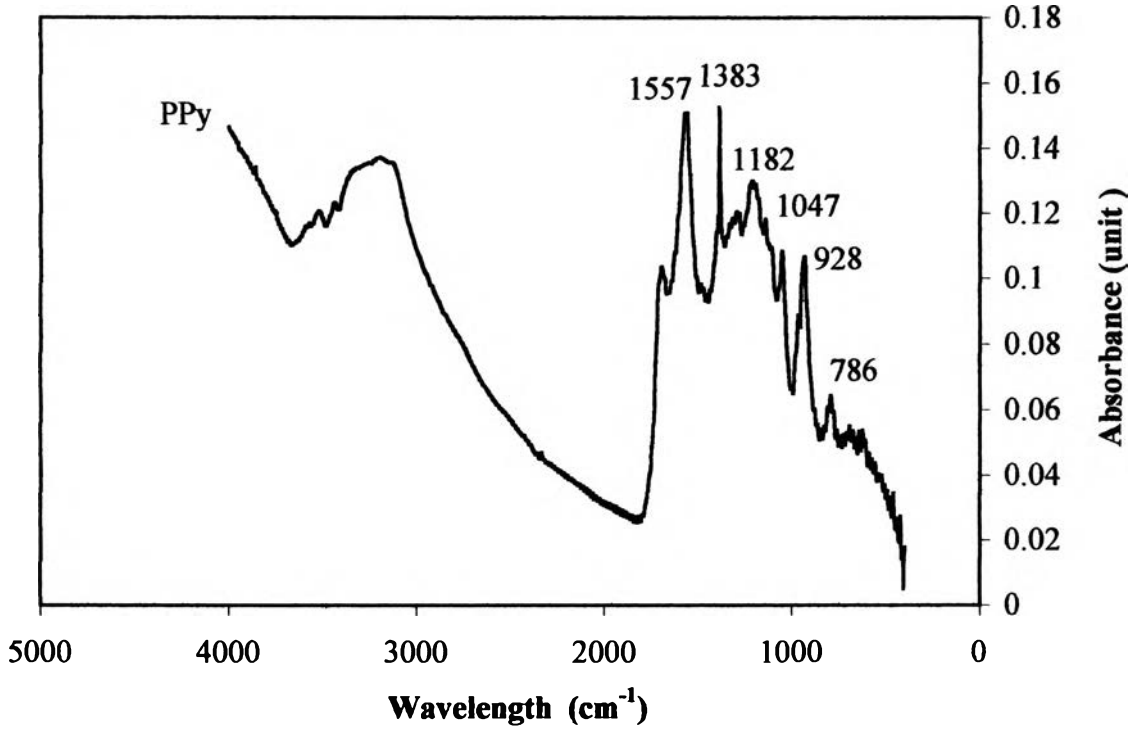

Figure 4.13 FT-IR spectra of PPy.

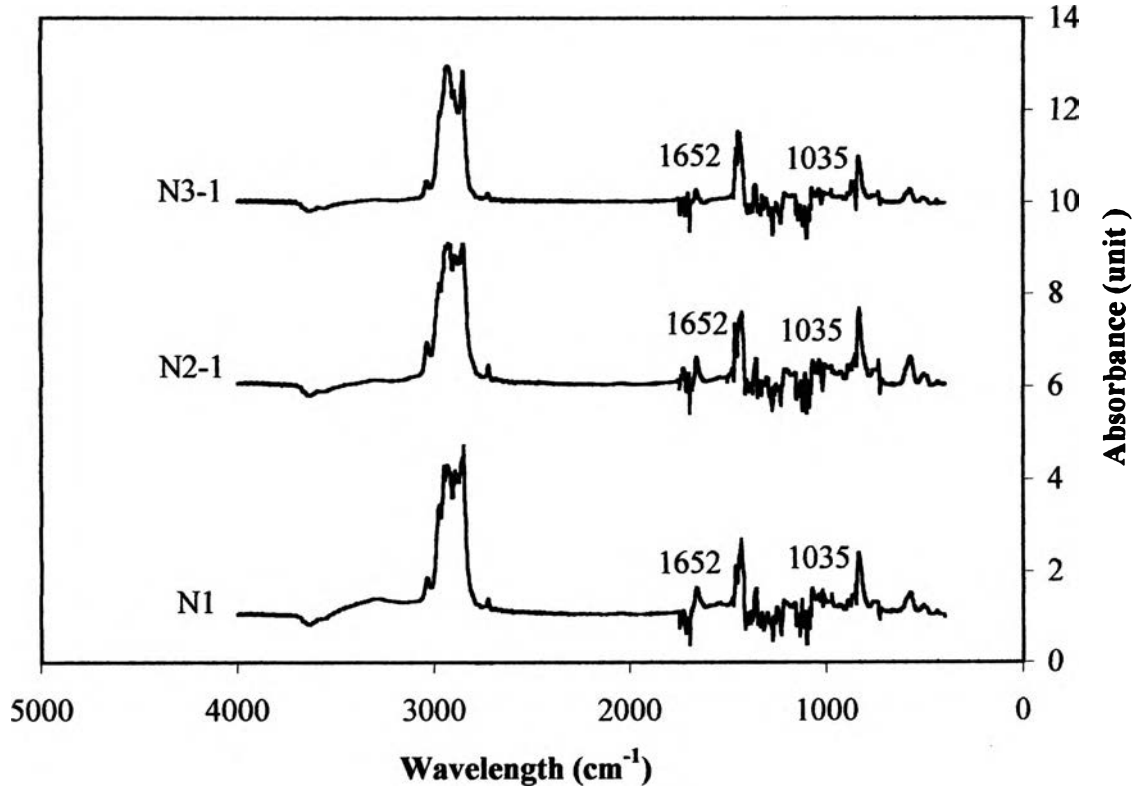

Figure 4.14 FT-IR spectra of admicelled latex film.

4.7 Rheological Measurement

Frequency-sweep measurements were performed at a given stress (chosen in the linear viscoelastic region where the amplitude of the deformations is very low) in the frequency (ω) region range from 0.1-100 rad/s. The storage and loss moduli of NR and admicelled latex plotted against the angular frequency are shown in Figure 4.15. It can be seen that storage modulus increases gradually with increasing angular frequency. The influence of pyrrole concentration on rheological parameters of the admicelled latices is presented. Sample N2-3 has the highest G' while all admicelled latices gained an improvement in G' (ranging between $3x10^4$ and $6x10^4$ Pa) compared with NR latex and N1 ($1.3x10^4$ and $1.5x10^4$ Pa, respectively). The reinforcement effect of N3 series was not greater than N2 while N1 had small reinforcement effect after the polymerization. This suggests better compatibility by admicellar polymerization than simple mixing. It appears that at high PPy content, N2-4 and N3-3 has less G' and G" due to inhomogenuity. In Figure 4.16, the loss modulus (G") shows similar trend as G'. High G" related to high viscous part of admicelled latex samples suggests that their deformation cause intensive energy dissipation. N2 system shows higher and more fluctuation of G" than N3 samples due to more heterogeneity. These results suggest that tan δ (G"/G') of the admicelled latices is in the range of processable with moderate viscosity as seen in Figure 4.17. Tan δ of the admicelled latex samples are slightly less than those of NR and N1 suggesting that they are processable somewhat like NR. By dynamic mechanical test, the complex viscosity (η^*) curves, depicted in Figure 4.18 shows a shear thinning behavior in the frequency range from 0.1-100 rad/s. Complex viscosity of the admicelled latex samples has higher viscosity than pure NR and N1. There is no significant difference in viscosity of N2 and N3 samples. The viscosity range of admicelled latex films are $2.77x10^5$ to $3.81x10^5$ Pa-s or greater by 2 times than that of NR.

Although SEM results imply that N3 samples have more PPy admicellar polymerization than N2 samples as evident by denser deposition of new PPy from two-step polymerization on the coated latex. Storage moduli of N3 samples are lower than those of N2 samples and reduce with pyrrole content in opposite to N2 where G' is increases with PPy content. This can contribute to more inhomogeneous texture of N3 with more rigid PPy agglomerates than N2 such that those rigid agglomerates become brittle leading to early breakage.

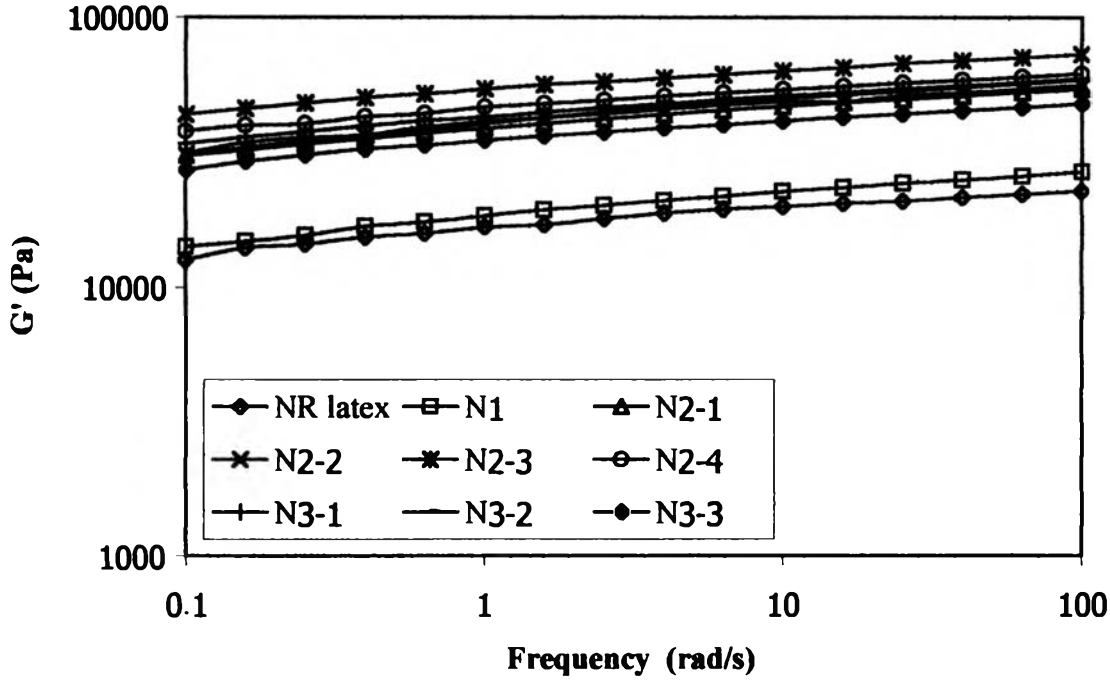

Figure 4.15 Storage moduli (G') of admicelled latex films compared to pure NR latex (no oxidant) and N1 film 70^{0}C.

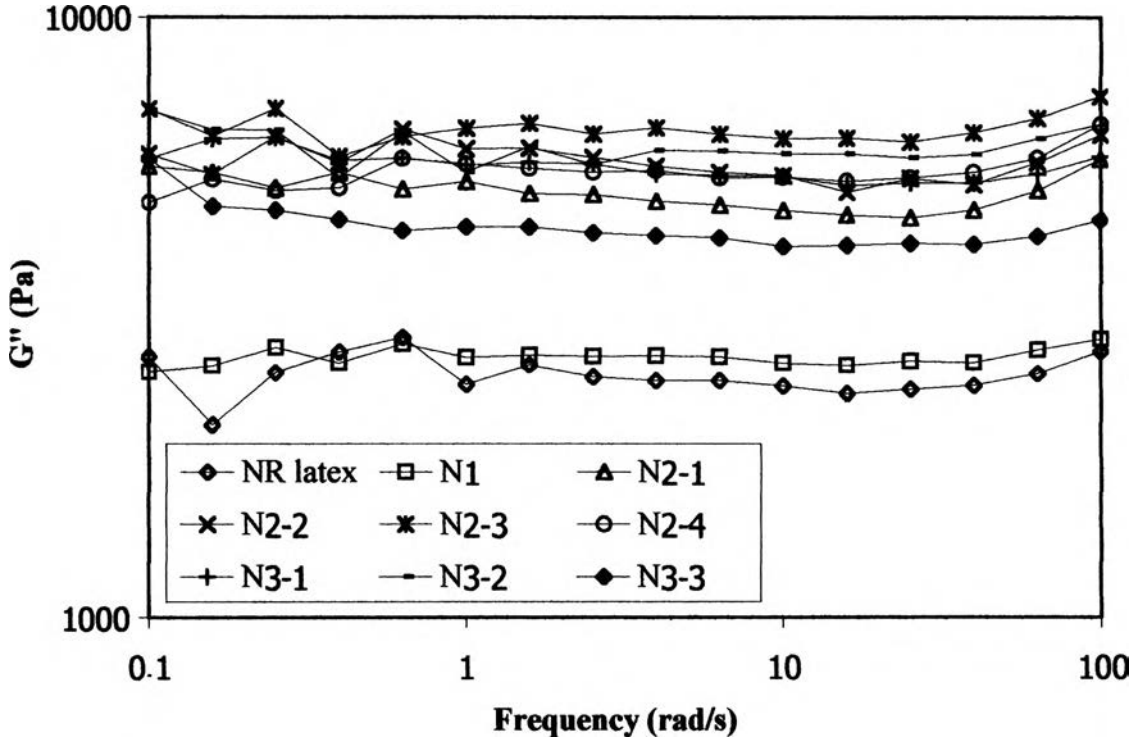

Figure 4.16 Loss moduli (G") of admicelled latex films compared to pure NR latex and N1 film at 70^0C.

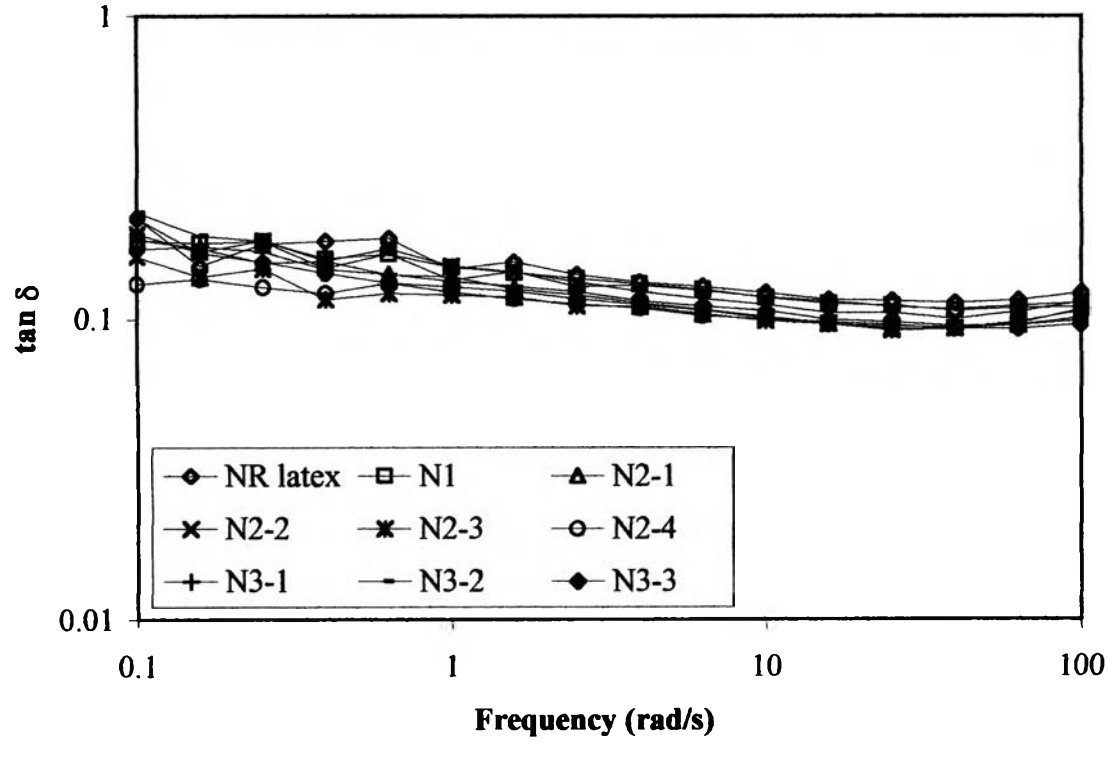

Figure 4.17 Tan δ of admicelled latex films compared to pure NR latex and N1 film 70^0C.

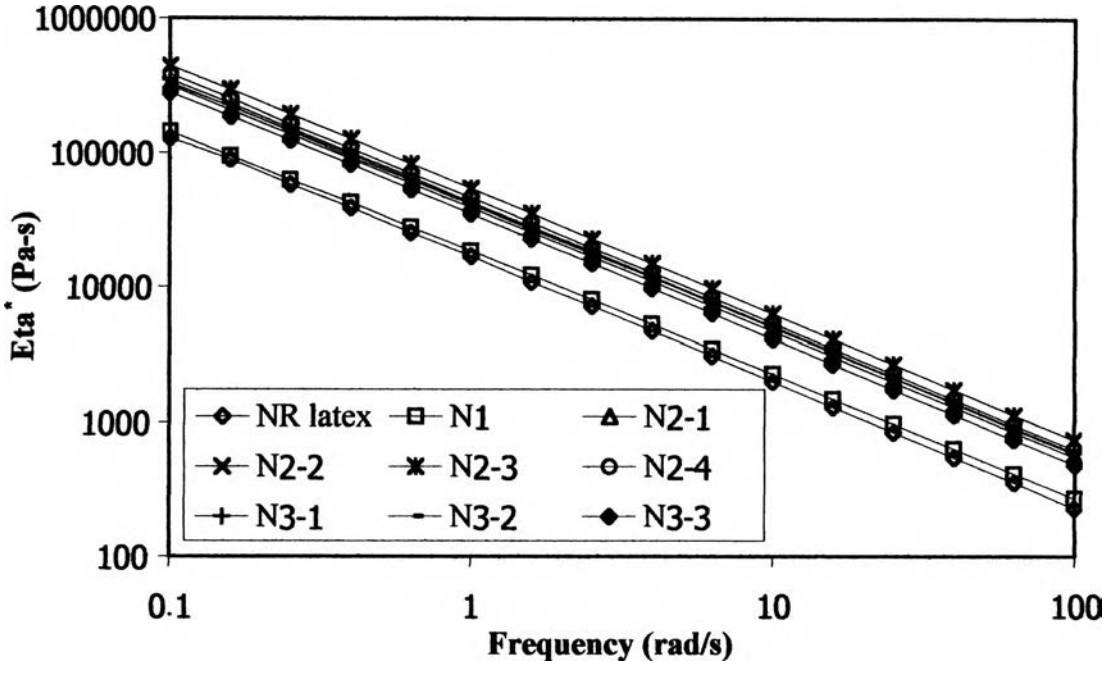

Figure 4.18 Complex viscosity (η^*) of admicelled latex films compared to pure NR latex and N1 film 70^0C.

4.8 Mechanical Properties Measurement

The effect of pyrrole concentration on the mechanical properties of admicelled latices shown in Figures 4.19-4.22 indicates that tensile properties of N2-3 and N3-3 which contained pyrrole concentration of 20 mM provided the highest mechanical properties. There were no significant changes in the properties of NR, N1, Ctrl. 1, and Ctrl. 2. However, a slight increase in these properties was obtained for N2-2A9P1 containing 10 wt% of pyrrole. Of all the samples, N3-3 provided the best properties in mechanical testing because of the highest pyrrole concentration (~ 5 wt% of pyrrole) and salt addition. It is interesting to note that admicelled latices provided superior elongation and strength much better than pristine NR and hardly seen in most polymers. This may be due to good adhesion and inclusion morphology like those found in SBS or rubber toughen copolymers.

Li and Ouyang (2000) prepared PPy with non-ionic surfactant varying polyethyleneoxy ether (OP) length between 4-21 units by electropolymerization. They successfully obtained high conductivity of >90 S/cm, high tensile strength greater than 64 MPa and elongation at break about 16-20% when OP greater than 10 units was used. Yin *et al.* (1998, 1997) also got good mechanical strength (6.2 MPa and 10.3 MPa) and elongation at break (94.7% and 170%) for composites of PPy and crosslinked poly(styene/butyl acrylate/acrylic acid) copolymer with tetraethylorthosilicate as a crosslinker. On the other hand, Bhat *et al.* (1995) claimed large reduction in tensile strength and elongation at break with increased PPy content due to strong tie molecules between PPy and PVDF phases.

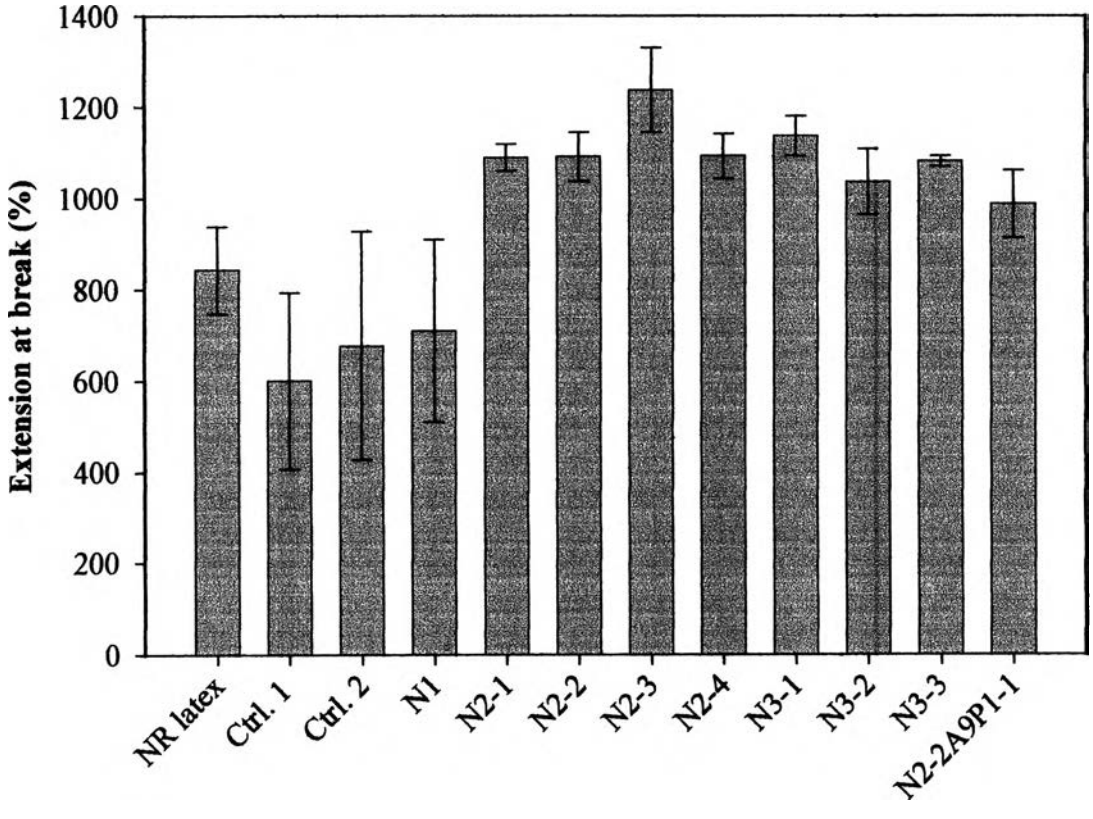

Figure 4.19 %extension at break of admicelled latex samples compared with pure NR latex. Crosshead speed = 500 mm/min, grip separation = 50 mm.

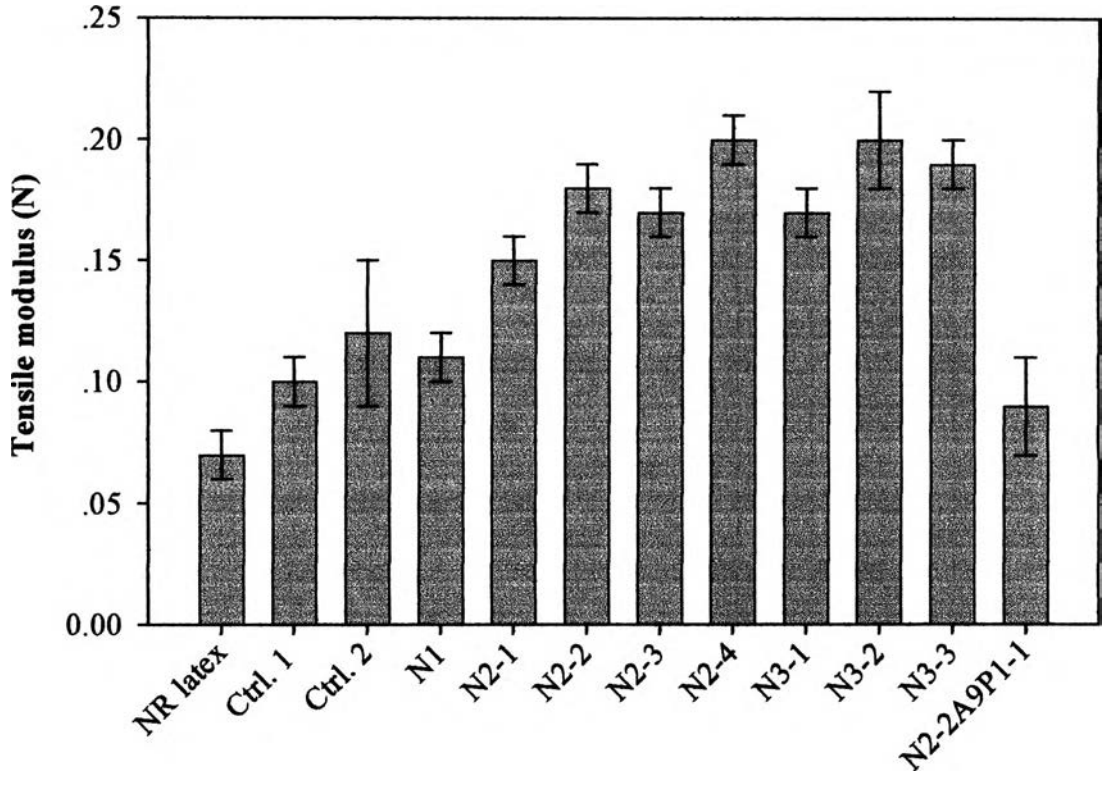

Figure 4.20 Tensile modulus of admicelled latex samples compared with pure NR latex. Crosshead speed = 500 mm/min, grip separation = 50 mm.

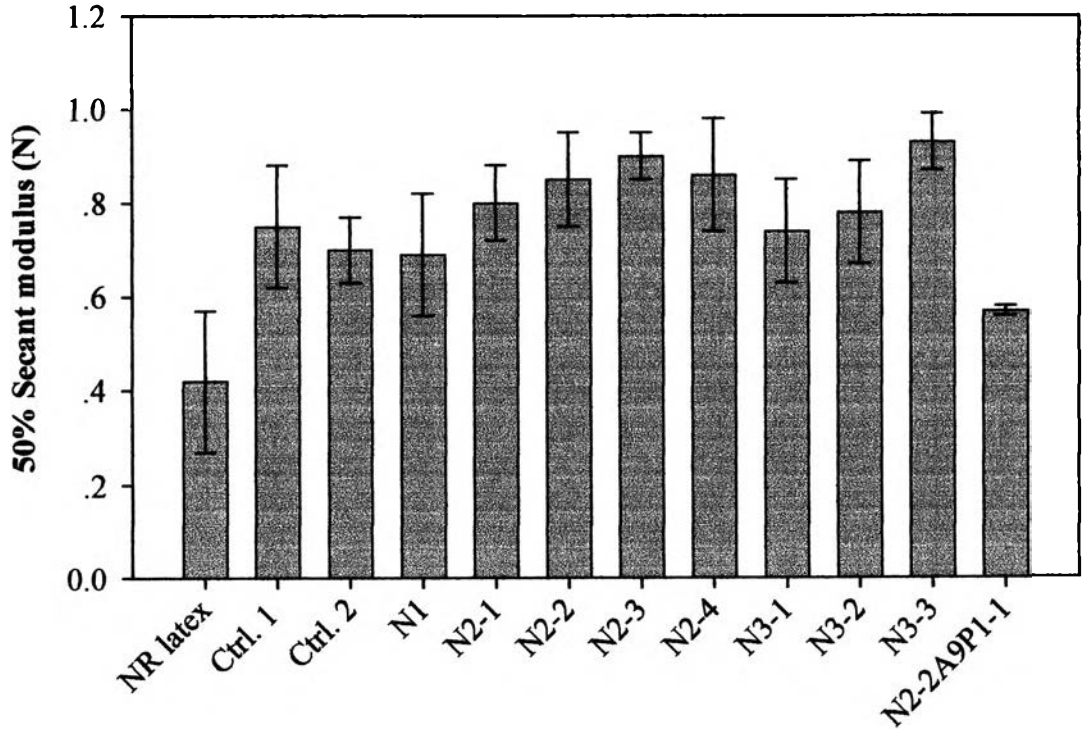

Figure 4.21 50% secant modulus of admicelled latex samples compared with pure NR latex. Crosshead speed = 500 mm/min, grip separation = 50 mm.

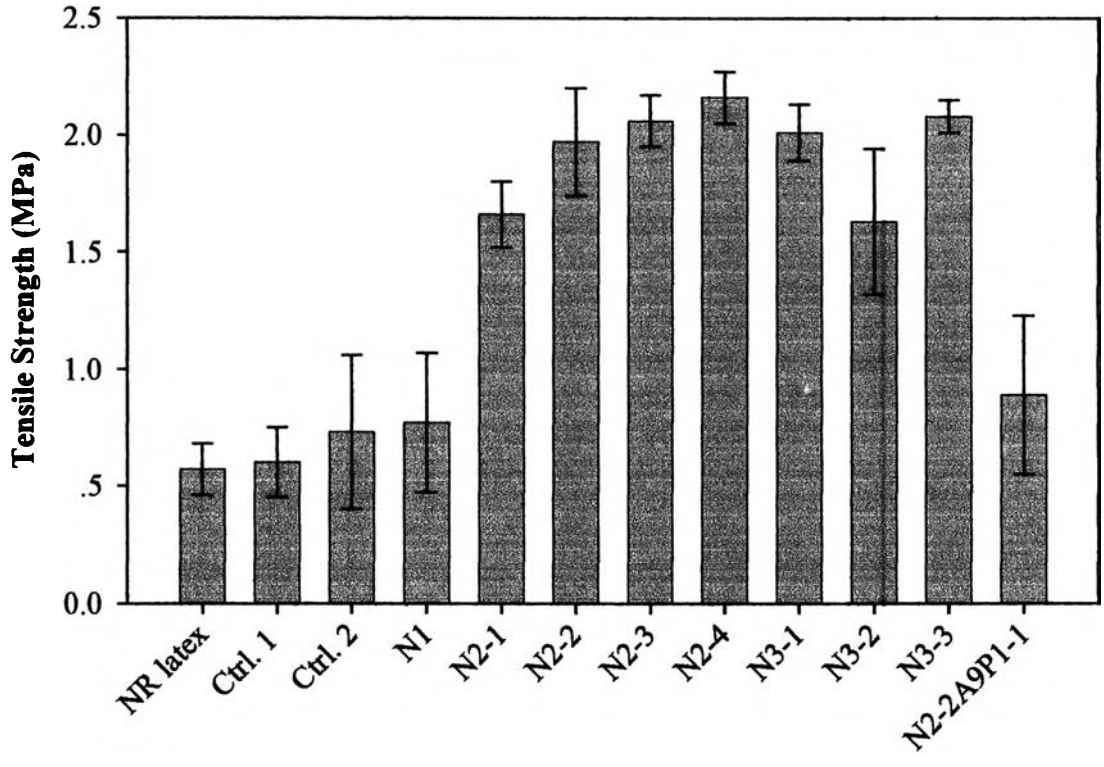

Figure 4.22 Tensile strength of admicelled latex samples compared with pure NR latex. Crosshead speed = 500 mm/min, grip separation = 50 mm

Table 4.3 Mechanical properties of various admicelled latex films

Sample	Extension @ break (%)	Tensile Modulus (N)	Tensile Strength (MPa)	50% secant modulus (N)
NR latex*	842.54±95.64	0.07±0.01	0.57±0.11	0.42±0.15
Ctrl. 1	599.90±192.86	0.10±1.01	0.60±0.15	0.75±0.13
Ctrl. 2	676.86±370.04	0.12±0.03	0.73±0.33	0.70±0.07
N1	709.90±199.99	0.11±0.01	0.77±0.30	0.69±0.13
N2-1	1089.20±29.63	0.15±0.01	1.66±0.14	0.80±0.08
N2-2	1090.60±53.62	0.18±0.01	1.97±0.23	0.85±0.10
N2-3	1237.60±93.14	0.17±0.01	2.06±0.11	0.90±0.05
N2-4	1092.00±48.90	0.20±0.01	2.16±0.11	0.86±0.12
N3-1	1136.40±43.67	0.17±0.01	2.01±0.12	0.74±0.11
N3-2	1036.04±71.86	0.20±0.10	1.63±0.31	0.78±0.11
N3-3	1080.80±12.24	0.19±0.00	2.08±0.07	0.93±0.06
N2-2A9P1-1	986.44±74.04	0.09±0.02	0.89±0.34	0.57±0.01

* No $(NH_4)_2S_2O_8$

4.9 Conductivity Measurement

Table 4.4 represents the surface resistivity of various admicelled latices at different pyrrole concentrations. The sample with no admicellar treated has the highest conductivity at around 2.103×10^{-10} Ω^{-1} and the samples with adding salt have higher conductivity than those samples without salt. These results suggest that the conductivity of the latices improved after admicellar polymerization. Both N2 and N3 with more PPy shows increasing conductivity; heterogeneity likely causes slight reduction in conductivity whereas the heterogeneous N1 turns to exhibit strong conductivity. The reason is unclear. In comparison, N3 shows better conductivity than N2 with increasing PPy content.

The core-shell particles showed increased conductivity with increasing PPy content but less stability leading to flocculation (Huijs *et al.*, 2001 and Lascelles and

Armes, 1997). Omastova *et al.* (1998) reported the blends of PPy coated PMMA particles and PMMA showed higher conductivity (10^{-3} S/cm at PPy 3.5 wt% or >30 wt% of coated PMMA) than the PPy coated PMMA composite (10^{-7} S/cm at PPy 3.5 wt%) about 4 decades at all composition of PPy (0-5 wt%). This was due to percolation (network formed) was reached and the superstructure of the PPy coated PMMA. Crosslink of the PMMA core did not alter the conducitivity. Lascelles and Armes, 1997 reported the same trend that percolation threshold of core-shell type PPy coated PS was much lower (5 vol% PPy) than the heterogeneous PPy powder/PS composite (20 vol% PPy).

Table 4.4 Surface resistivity and conductivity (S) of the admicelled latices at various pyrrole concentration

Samples	Surface resistivity (Ω)	Conductivity (Siemen)
NR latex*	$1.278\text{x}10^{14} \pm 0.291\text{x}10^{14}$	$7.825\text{x}10^{-15} \pm 3.436\text{x}10^{-14}$
Ctrl. 1	$4.486\text{x}10^{11} \pm 0.027\text{x}10^{11}$	$2.223\text{x}10^{-12} \pm 3.704\text{x}10^{-10}$
Ctrl. 2	$4.648\text{x}10^{14} \pm 0.518\text{x}10^{14}$	$2.151\text{x}10^{-15} \pm 1.931\text{x}10^{-14}$
N1	$2.103\text{x}10^{10} \pm 0.283\text{x}10^{10}$	$4.755\text{x}10^{-11} \pm 3.534\text{x}10^{-10}$
N2-1	$3.766\text{x}10^{14} \pm 0.204\text{x}10^{14}$	$2.655\text{x}10^{-15} \pm 4.902\text{x}10^{-14}$
N2-2	$1.290\text{x}10^{14} \pm 0.520\text{x}10^{14}$	$7.752\text{x}10^{-15} \pm 1.923\text{x}10^{-14}$
N2-3	$7.771\text{x}10^{13} \pm 0.430\text{x}10^{13}$	$1.287\text{x}10^{-14} \pm 2.326\text{x}10^{-13}$
N2-4	$5.355\text{x}10^{13} \pm 0.471\text{x}10^{13}$	$1.867\text{x}10^{-14} \pm 2.123\text{x}10^{-13}$
N3-1	$2.757\text{x}10^{13} \pm 0.568\text{x}10^{13}$	$3.627\text{x}10^{-14} \pm 1.761\text{x}10^{-13}$
N3-2	$2.174\text{x}10^{13} \pm 0.112\text{x}10^{13}$	$4.600\text{x}10^{-14} \pm 8.929\text{x}10^{-13}$
N3-3	$2.005\text{x}10^{13} \pm 0.280\text{x}10^{13}$	$4.988\text{x}10^{-14} \pm 3.571\text{x}10^{-13}$

* No $(NH_4)_2S_2O_8$

Samples from 2-step process can not be measured the resistivity because of their rough surface.